European Journal of Mechanics / A Solids 114 (2025) 105737

Contents lists available at ScienceDirect

European Journal of Mechanics / A Solids

journal homepage: www.elsevier.com/locate/ejmsol

Full Length Article

# A modified low cycle fatigue Chaboche model for irradiation hardening behaviour of EUROFER97 at elevated temperatures

Jianxin Liu [a], Xiaowei Wang [b,c], Aleksandr Zinovev [d], Dmitry Terentyev [d], Lihua Wang [e,*], Magd Abdel Wahab [a,f,g,**]

[a] Soete Laboratory, Department of Electrical Energy, Metals, Mechanical Constructions and Systems, Faculty of Engineering and Architecture, Ghent University, 9000, Ghent, Belgium
[b] School of Mechanical and Power Engineering, Nanjing Tech University, Nanjing, 211816, China
[c] Reliability Centered Manufacturing Research Institute, Nanjing Tech University, Nanjing, 211816, China
[d] Structural Materials Group, Institute for Nuclear Energy Technology, Belgian Nuclear Research Centre SCK CEN, 2400, Mol, Belgium
[e] School of Aerospace Engineering and Applied Mechanics, Tongji University, Shanghai, 200092, China
[f] Parallel and Distributed Systems Laboratory, Jožef Stefan Institute, Jamova cesta 39, SI-1000, Ljubljana, Slovenia
[g] College of Engineering, Yuan Ze University, Taiwan, Republic of China

ARTICLE INFO

*Keywords:*
Irradiation hardening
Mechanical behaviour
EUROFER97
Low cycle fatigue
Finite element analysis

ABSTRACT

This study investigates the irradiation hardening mechanical behaviour of EUROFER97, a Reduced Activation Ferritic/Martensitic (RAFM) steel, using a modified Chaboche model within the temperature range of 250–350 °C. Structural materials for nuclear fusion reactors must maintain their performance under neutron irradiation. However, EUROFER97 faces challenges such as irradiation-induced hardening and embrittlement at irradiation temperatures below 350 °C, which lead to reduced ductility and toughness. This research incorporates an irradiation hardening factor into a modified Chaboche constitutive model to accurately simulate EUROFER97's behaviour under irradiation. A unified viscoplastic model is employed for finite element analysis, with variable parameters used to better represent the material's stress-strain evolution during cyclic loading and irradiation-induced hardening. Simulations are conducted using ABAQUS, with a UMAT subroutine developed to simulate fatigue, and a hybrid acceleration strategy is adopted to accelerate the calculation of different stages of Low Cycle Fatigue (LCF). Key findings demonstrate that the modified Chaboche model effectively predicts the irradiation hardening and cyclic softening behaviour of EUROFER97 under various irradiation doses and strain amplitudes. The model's predictions are in good agreement with experimental data, capturing the stress-strain hysteresis loops and irradiation-induced changes in mechanical properties, thereby validating its applicability not only to EUROFER97 but also to other nuclear structural materials, such as F82H ferritic/martensitic steel. The contribution of this study lies in refining the Chaboche model by incorporating irradiation effects, providing a robust tool for predicting the mechanical behaviour of structural materials under irradiation, which is crucial for the safety and design of fusion reactor components.

## 1. Introduction

Nuclear fusion is increasingly recognized as a highly promising source of clean and sustainable energy (Bodel et al., 2021). Nevertheless, the commercialization of fusion reactors poses numerous technical challenges, particularly in the development of structural materials capable of maintaining long-term stability under harsh irradiation conditions. Key components of fusion reactors, such as the first wall and blanket, are subjected to significant thermal loads and intense neutron irradiation, leading to material failure characterized by phenomena such as irradiation hardening, embrittlement, swelling, irradiation-induced creep, phase changes, and the formation of gas bubbles. These effects collectively compromise the mechanical properties, dimensional stability, and structural integrity of the materials,

* Corresponding author.
** Corresponding author. Soete Laboratory, Department of Electrical Energy, Metals, Mechanical Constructions and Systems, Faculty of Engineering and Architecture, Ghent University, 9000, Ghent, Belgium.
*E-mail addresses:* lhwang@tongji.edu.cn (L. Wang), magd.abdelwahab@ugent.be (M. Abdel Wahab).

https://doi.org/10.1016/j.euromechsol.2025.105737
Received 19 November 2024; Received in revised form 25 March 2025; Accepted 26 May 2025
Available online 27 May 2025
0997-7538/

challenging the long-term durability and safety of reactor components (Windsor et al., 1999; Bhattacharya et al., 2022). Therefore, advancing high-performance structural materials for fusion reactors is crucial to ensuring their safe and reliable operation.

Among the candidate materials, Reduced Activation Ferritic/ Martensitic (RAFM) steels are prominent due to their exceptional resistance to irradiation, strong high-temperature performance, good thermal conductivity, and low levels of activation after irradiation (Zinkle et al., 2017). EUROFER97, developed in Europe as a leading RAFM steel, has been extensively studied and applied in fusion material research (Gaganidze et al., 2018; Tavassoli et al., 2014). This alloy demonstrates excellent mechanical properties and resistance to irradiation-induced swelling in the operational temperature range of 350 °C–550 °C (Melton et al., 2020). However, at lower temperatures (particularly between 250 °C and 350 °C) (Materna-Morris et al., 2013), EUROFER97 experiences significant irradiation hardening and embrittlement, resulting in reduced ductility and fracture toughness. These effects restrict the application scope of EUROFER97 steel and pose a substantial challenge to the structural integrity of components (Cabet et al., 2019; Bhattacharya et al., 2021).

Accurate prediction and understanding of material property changes under irradiation are vital for the design and safety evaluation of fusion reactors. Robust constitutive models are essential for providing engineers with reliable predictions of material behaviour, facilitating optimized design and extended component lifetimes. However, the complex microstructural changes induced by irradiation significantly influence mechanical behaviour, complicating the development of comprehensive constitutive models (Aktaa and Petersen, 2011; Aktaa and Petersen, 2009a; Aktaa and Petersen, 2009b; Deo et al., 2008; Frydrych).

Multi-scale simulation methods have been extensively employed in the constitutive modelling of irradiated materials. These approaches encompass a spectrum of computational techniques, ranging from atomic-scale Molecular Dynamics (MD) simulations to grain-scale Discrete Dislocation Dynamics (DDD), and extending up to macroscopic finite element analyses (Bacon and Osetsky, 2002; Lin et al., 2024; Marian et al., 2020; Khraishi et al., 2002; Reali and Dudarev, 2024). The primary objective is to bridge micro-scale defect behaviours with macro-scale mechanical properties, thereby providing a comprehensive understanding across different length scales. This multi-scale methodology enables more accurate predictions of material responses under complex irradiation environments. However, the substantial computational resources required for such detailed simulations limit their practical application in large-scale engineering contexts (Van Der Giessen et al., 2020). As a result, phenomenological constitutive models, which are based on experimental data and incorporate empirical parameters to describe material stress-strain relationships, are more commonly utilized. By integrating irradiation effects into these macro-scale phenomenological models, the predictive accuracy regarding material behaviour under irradiation can be significantly enhanced. Among these, the Chaboche constitutive model, a nonlinear cyclic plasticity framework, has proven particularly valuable for studying the mechanical properties of metallic materials. Known for its robustness in capturing complex behaviours such as cyclic hardening/softening, and stress relaxation, the Chaboche model provides a practical approach for simulating cyclic loading conditions and predicting material responses with high accuracy (Zhang and Aktaa, 2020; Zhang and Xuan, 2017).

This paper introduces an irradiation hardening factor to refine specific parameters within the modified Chaboche constitutive model (Wang et al., 2021), significantly enhancing the model's ability to predict material behaviour under irradiation conditions. The modified model effectively captures stress-strain evolution during complex cyclic loading (Zahran et al., 2024). By incorporating the irradiation hardening factor, the model accounts for both cyclic softening and irradiation hardening effects, enabling a more accurate representation of Eurofer97's behaviour under various irradiation doses. Simulations of fatigue tests were conducted using ABAQUS with a UMAT subroutine, while a hybrid acceleration strategy was employed to expedite the calculations of different stages of Low Cycle Fatigue (LCF). The key findings demonstrate that the modified Chaboche model effectively predicts the irradiation hardening and cyclic softening behaviours of EUROFER97 under different irradiation doses and strain amplitudes. This advancement not only enhances simulation accuracy but also provides a stronger theoretical foundation for the structural design and life assessment of materials in irradiation environments.

## 2. Modelling and simulation

This study introduces an irradiation hardening factor into the modified Chaboche unified viscoplastic model by Wang et al. (2021) to accurately simulate the time-dependent LCF behaviour of EUROFER97 steel under both irradiated and unirradiated conditions in finite element analysis. The Wang's model was selected for comparison with the traditional Chaboche model because it introduces variable parameters in the kinematic hardening component, which significantly enhances the accuracy of stress relaxation simulations. This modification enables the model to more precisely capture the stress-strain evolution of the material under complex cyclic loading, particularly in the stress relaxation and cyclic plastic deformation phases. These advancements not only improve simulation accuracy but also provide a more reliable tool for predicting the mechanical behaviour of EUROFER97 steel in irradiation environments.

### 2.1. Overview of constitutive model

Under isothermal conditions, the total strain $\boldsymbol{\varepsilon}_{\text{total}}$ in the unified viscoplastic constitutive model is expressed by Equation (1):

$$\boldsymbol{\varepsilon}_{\text{total}} = \boldsymbol{\varepsilon}_{\text{e}} + \boldsymbol{\varepsilon}_{\text{in}} \tag{1}$$

Here, $\boldsymbol{\varepsilon}_{\text{e}}$ and $\boldsymbol{\varepsilon}_{\text{in}}$ represent the elastic strain and inelastic strain, respectively. Combining Hooke's law with Equation (1), the stress $\boldsymbol{\sigma}$ can be expressed as:

$$\boldsymbol{\sigma} = \mathbf{E} : (\boldsymbol{\varepsilon}_{\text{total}} - \boldsymbol{\varepsilon}_{\text{in}}) \tag{2}$$

where $\mathbf{E}$ is the elastic stiffness matrix. By selecting the yield function as the plastic potential function and applying the associated flow rule, the rate of inelastic strain is given by:

$$\dot{\boldsymbol{\varepsilon}}_{\text{in}} = \dot{p}\cdot\frac{\partial f_y}{\partial \boldsymbol{\sigma}} = \frac{3}{2}\dot{p}\cdot\frac{\boldsymbol{\sigma}' - \boldsymbol{\chi}'}{J(\boldsymbol{\sigma} - \boldsymbol{\chi})} \tag{3}$$

Here, $\dot{\boldsymbol{\varepsilon}}_{\text{in}}$ denotes the rate of the inelastic strain tensor; $\dot{p} = \dot{\bar{\varepsilon}}_{\text{in}}$ is the plastic multiplier and equals to the equivalent inelastic strain rate, which is the derivative of the accumulated inelastic strain $p$ with respect to time and can be expressed by Equation (4). The yield function $f_y$, based on the von-Mises yield criterion, is expressed by Equation (5), where $\boldsymbol{\sigma}$ and $\boldsymbol{\chi}$ represent the stress tensor and the back stress tensor, respectively. The superscript ($'$) denotes their deviatoric components; $J(\boldsymbol{\sigma} - \boldsymbol{\chi})$ represents the second invariant, calculated as shown in Equation (6):

$$\dot{p} = \langle \frac{f_y}{Z} \rangle^n \tag{4}$$

$$f_y = J(\boldsymbol{\sigma} - \boldsymbol{\chi}) - (y_0 + R) \tag{5}$$

$$J(\boldsymbol{\sigma} - \boldsymbol{\chi}) = \left[\frac{3}{2}(\boldsymbol{\sigma}' - \boldsymbol{\chi}') : (\boldsymbol{\sigma}' - \boldsymbol{\chi}')\right]^{\frac{1}{2}} \tag{6}$$

In these equations, $\langle\rangle$ is the Macaulay notation, defined as $\langle x \rangle = (|x| + x)/2$; $Z$ and $n$ are material-related viscous coefficients and viscous exponents, respectively. $y_0$ and $R$ are the initial yield stress and isotropic hardening variable and the operator ( : ) denotes the double contraction of tensors (also known as the double dot product).

- Non-linear Kinematic Hardening Equation

The non-linear kinematic hardening equation proposed by Wang et al. is adopted, where the evolution of the back stress is described by the following equations:

$$\boldsymbol{\chi} = \boldsymbol{\chi}_1 + \boldsymbol{\chi}_2 \tag{7}$$

$$\dot{\boldsymbol{\chi}}_1 = \xi_1 \cdot \left( \frac{2}{3}\gamma_1 \cdot \dot{\boldsymbol{\varepsilon}}_{\mathrm{in}} - \boldsymbol{\chi}_1 \cdot \dot{p} \right) \tag{8}$$

$$\dot{\boldsymbol{\chi}}_2 = \xi_2 \cdot \left[ \frac{2}{3}\gamma_2 \cdot \dot{\boldsymbol{\varepsilon}}_{\mathrm{in}} - \mu(p) \cdot \boldsymbol{\chi}_2 \cdot \dot{p} \right] - \tau(p) \cdot [J(\boldsymbol{\chi}_2)]^{m-1} \cdot \boldsymbol{\chi}_2 \tag{9}$$

In these equations, $\boldsymbol{\chi}_1$ and $\boldsymbol{\chi}_2$ describe the hardening behaviour at the initial stage and the stage when the strain is relatively large during the later period, respectively. $\xi_1, \xi_2, \gamma_1, \gamma_2, m$ are material-related constants. Xuan et al. (Zhang and Xuan, 2017) modified the material constant $\tau_0$ in the traditional Chaboche constitutive model to a variable $\tau(p) = \tau_0[\phi + (1-\phi) \cdot e^{-\omega \cdot p}]$. On this basis, Wang added a dynamic parameter $\mu(p) = 1 + \lambda \cdot (1 - e^{-\delta \cdot p})$, where $\phi$, $\omega$, $\lambda$ and $\delta$ are material constants. These improvements enable the model to more accurately describe the evolution of back stress and hardening behaviour of materials during cyclic loading.

- Isotropic Hardening Equation

The following isotropic hardening equation is used to describe the evolution of the hardening variable $R$:

$$\dot{R} = b \cdot (Q - R) \cdot \dot{p} \tag{10}$$

The parameter $b$ represents the rate at which the isotropic hardening variable $R$ reaches the saturation value $Q$. This equation can capture the saturation phenomenon in the material hardening process, corresponding to the gradually stabilized hardening behaviour of the material during cyclic loading.

- Irradiation Induced Hardening Equation

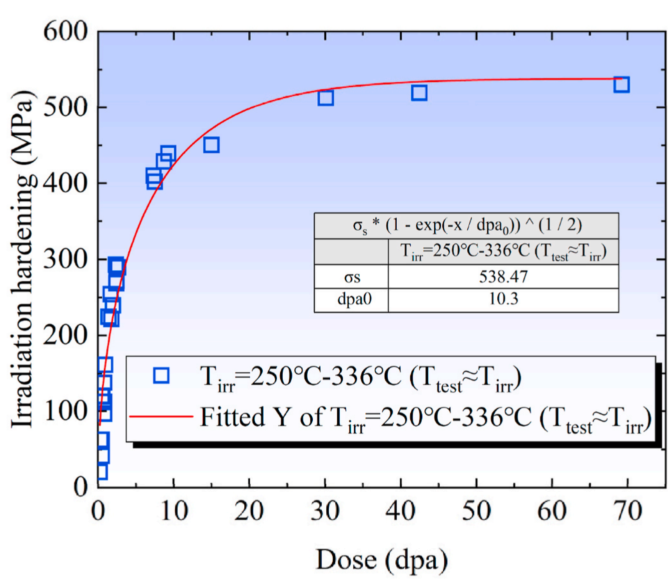


**Fig. 1.** Relationship between irradiation hardening and irradiation dose for EUROFER97 (Aktaa and Petersen, 2009b; Lucon and Vandermeulen; Gaganidze et al.; Aktaa and Petersen, 2009c).

As shown in Fig. 1, a nonlinear irradiation hardening relationship was introduced to accurately characterize the complex effects of irradiation hardening on the mechanical properties of the material (Yamamoto et al., 2006; Makin and Minter, 1960; Makin et al., 1962). The additional stress increment $\Delta\sigma_{\mathrm{irr}}$ induced by irradiation can be expressed as a function of irradiation dose $dpa$:

$$\Delta\sigma_{\mathrm{irr}} = \sigma_s \cdot \sqrt{1 - \exp\left( -\frac{dpa}{dpa_0} \right)} \tag{11}$$

Here, $\sigma_s$ is the saturation value of irradiation hardening, and $dpa_0$ is constant related to the material and irradiation conditions. This model reflects the influence of increasing irradiation dose on the strength of the material, exhibiting the saturation trend of irradiation hardening. When the irradiation dose $dpa$ is large, $\Delta\sigma_{\mathrm{irr}}$ approaches $\sigma_s$, indicating that the irradiation hardening effect of the material tends to saturate.

Under irradiation, the microstructure of the material undergoes changes, leading to the formation of dislocation obstacles, such as defects, vacancy clusters, and interstitial atom loops (Xiao, 2019). These obstacles impede dislocation movement, resulting in material hardening, which manifests as changes in yield stress and hardening behaviour. To quantitatively describe the irradiation-induced hardening effect, the irradiation hardening factor $H$ is introduced (Cho et al., 2021):

$$H = \frac{\Delta\sigma_{\mathrm{irr}}}{\sigma_{\mathrm{F}}} + 1 \tag{12}$$

According to Equation (12), the hardening factor $H$ characterizes the increase in hardening due to irradiation by expressing the ratio between the irradiation-induced hardening increment $\Delta\sigma_{\mathrm{irr}}$ and the steady-state hardening strength $\sigma_{\mathrm{F}}$ of an unirradiated (reference) material under the same thermomechanical conditions. This factor provides a measure of the relative enhancement in hardening resulting from irradiation effects. In this study, the relationship between the hardening effect and the irradiation dose, the sole variable, is established.

Irradiation increases the initial yield stress of the material. This is because high-energy particles generated during the irradiation process interact with the material, producing numerous point defects (vacancies and interstitial atoms) and more complex defect structures, such as dislocation loops and voids. These irradiation-induced defects obstruct dislocation motion, requiring higher stress for dislocation slip to overcome these obstacles, thus increasing the material's yield strength (Xiao, 2019). To account for the irradiation hardening effect, the initial yield stress is modified in the constitutive model as follows:

$$y_0^{\mathrm{irr}} = y_0 \cdot H \tag{13}$$

In this way, the effect of irradiation hardening on the yielding behaviour of the material is directly reflected in the yield criterion, allowing the model to simulate the actual mechanical response of the material under irradiation conditions. Additionally, irradiation also influences the kinematic hardening behaviour of materials, particularly the evolution of back stress. The defects induced by irradiation interact with mobile dislocations, altering the dislocation structure and distribution. This interaction can result in dislocation accumulation and changes in dislocation configurations, which in turn affect the magnitude and progression of back stress. Aligned with similar correction strategies, this simplification adjusts only the saturation value of kinematic hardening and the rate at which it is attained.

$$\gamma_i^{\mathrm{irr}} = \gamma_i \cdot H \tag{14}$$

$$\xi_i^{\mathrm{irr}} = \xi_i \cdot H \tag{15}$$

In Materna-Morris et al.'s study (Materna-Morris et al., 2011, 2013), a pronounced softening trend was observed in irradiated materials subjected to cyclic loading. The analysis revealed that dislocation loops and voids introduced by irradiation grow further and interact under cyclic stress, accelerating the accumulation of fatigue damage, which in turn leads to enhanced cyclic softening of the material. As a result, the saturation value describing isotropic hardening and the rate at which it is reached were modified as follows:

$$b_{irr} = b{\cdot}H, Q_{irr} = Q{\cdot}H \tag{16}$$

$$\dot{R}_{irr} = b_{irr} \cdot (Q_{irr} - R_{irr}){\cdot}\dot{p} \tag{17}$$

Finally, the yield function under irradiation is shown as:

$$f_y = J\left(\boldsymbol{\sigma} - \boldsymbol{\chi}_i^{irr}\right) - \left(y_0^{irr} + R_{irr}\right) \tag{18}$$

In summary, the improved constitutive model integrates nonlinear kinematic hardening, isotropic hardening, and irradiation-induced hardening effects, enabling more accurate simulation of EUROFER97 steel under complex loading and irradiation conditions.

**Table 1**
The material parameters of EUROFER97 at 250 °C in the unirradiated conditions.

| Parameter | Value | Units | Parameter | Value | Units |
|---|---|---|---|---|---|
| $E$ | 210.093 | GPa | $\nu$ | 0.3 | |
| $y_0$ | 199.69 | MPa | $\xi_1$ | 1507.3 | |
| $\xi_2$ | 172.5 | | $\gamma_1$ | 115.1 | MPa |
| $\gamma_2$ | 79.4 | MPa | $m$ | 2.89 | |
| $\tau_0$ | $2.84 \times 10^{-5}$ | $\text{MPa}^{1-m}/\text{s}$ | $Z$ | 380.6 | $\text{MPa}{\cdot}\text{s}^{1/n}$ |
| $n$ | 6.74 | | $\lambda$ | 0.085 | |
| $\delta$ | $2.55 \times 10^{-5}$ | | $\phi$ | 0.00883 | |
| $\omega$ | 18.798 | | $b$ | 2.383 | |
| $Q$ | −130 | MPa | $\sigma_s$ | 538.47 | MPa |
| $\sigma_F$ | 525.31 | MPa | $dpa_0$ | 10.30 | dpa |

## *2.2. Material parameter identification procedure*

The procedure for determining the material parameters is similar to that used in our previous work (Wang et al., 2021). As illustrated in the flowchart in Fig. 2, the identification process involves seven sequential steps. First, initial guesses for all material parameters are obtained following the step-by-step approach proposed by Tong et al. (2004). These values serve as the starting point for subsequent optimization. Second, experimental stress–strain data from the loading stage of the first cycle are used to estimate the elastic modulus $E$, the initial yield stress $y_0$, and the nonlinear kinematic hardening parameters $\xi i$ and $\gamma i$. Third, stress relaxation data from the first cycle are employed to identify the time-dependent viscoplastic parameters $Z$, $n$, $m$, $\tau_0$, based on the previously estimated parameters. In the fourth step, all these parameters are further optimized using the full hysteresis loop data from the first cycle. Fifth, with the optimized parameters from the previous step, the thermal recovery-related parameters $Z$, $n$, $m$, $\tau_0$, are calibrated using the evolution of relaxed stress as a function of cycle number. Sixth, the cyclic stress response curves are used to determine the isotropic hardening parameters $Q$ and $b$, independently of other variables. Finally, a global optimization is performed using multiple-cycle hysteresis loop data to ensure the consistency and accuracy of all identified parameters. In combination with Figs. 1 and 2, the final material parameters used in the constitutive model are summarized in Table 1. These parameters were derived based on experimental data and theoretical analysis to accurately capture the inelastic behaviour of EUROFER97 steel under both unirradiated and irradiated conditions.

The parameters listed in Table 1 (and Table 2 for F82H) correspond to the unirradiated condition, where the irradiation dose is assumed to be 0 dpa. These parameters are used in the constitutive Equations (1)–(11) to describe the baseline material behaviour. For irradiated conditions, the changes in material behaviour are modelled by introducing an irradiation hardening factor as defined in Equation (12). The relevant parameters (such as yield stress and hardening moduli) are then adjusted using this factor, as described in Equations (13)–(17), enabling a unified and consistent treatment of both irradiated and unirradiated conditions.

It is important to note that the material parameters identified through this procedure are not strain-amplitude specific. Instead, they are intended to be valid across a range of strain amplitudes, including those used in this study (±0.3 % and ±0.5 %). To ensure broad applicability, the calibration was performed using experimental data at a relatively high strain amplitude (Marmy, 2006), where both cyclic softening and stress relaxation are more pronounced. This approach

**Table 2**
The material parameters of F82H at room temperature in the unirradiated conditions.

| Parameter | Value | Units | Parameter | Value | Units |
|---|---|---|---|---|---|
| $E$ | 211.1 | GPa | $\nu$ | 0.3 | |
| $y_0$ | 430.09 | MPa | $\xi_1$ | 1500.3 | |
| $\xi_2$ | 169.5 | | $\gamma_1$ | 133.1 | MPa |
| $\gamma_2$ | 78.3 | MPa | $b$ | 2.58 | |
| $Q$ | −150 | MPa | $\sigma_F$ | 733.3 | MPa |

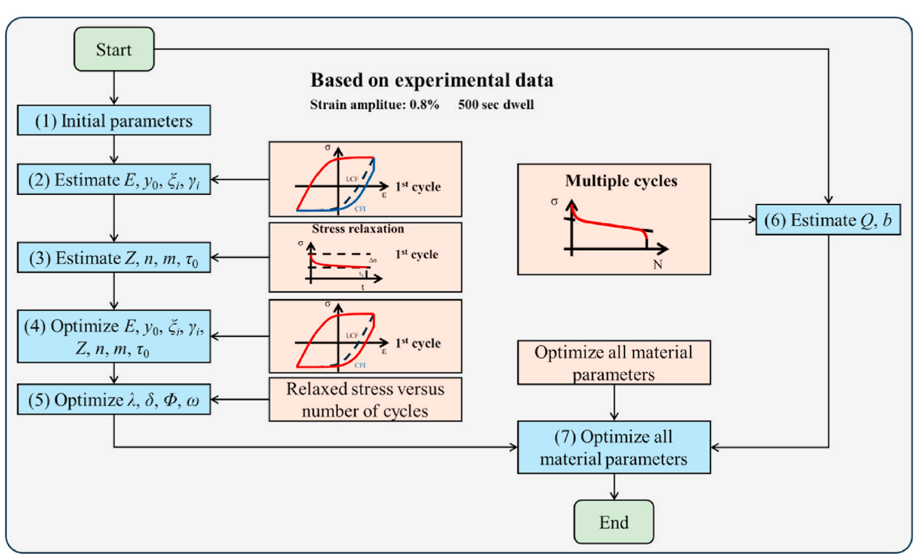


**Fig. 2.** Flowchart of the optimization procedure to determine material parameters.

enables the constitutive model to accurately reproduce the mechanical response under different loading amplitudes without requiring separate parameter sets for each case. The validity of this approach is further supported by previous studies in the field of cyclic plasticity modelling.

### 2.3. Implementation in numerical simulation

The aforementioned constitutive model was implemented into the UMAT subroutine of ABAQUS for finite element simulation analysis. The geometry of the component and the loading conditions are based on the study by Materna-Morris et al. (2011). Fig. 3 illustrates the cylindrical fatigue specimen model utilized in this study. The model was discretized using 4336 C3D8R elements, and the motion of the two end surfaces was constrained via coupling to reference points RP-1 and RP-2, ensuring appropriate boundary conditions. In the numerical simulation of LCF, a symmetric triangular strain waveform with a strain ratio of R = −1 is applied, as depicted on the right side of the figure. The loading was fully reversed and strain-controlled, consistent with the experimental setup. A strain rate of 0.1 mm/min is adopted to match the conditions used in the fully-instrumented tensile fatigue tests. The model is used to simulate the stress-strain hysteresis loops under different strain amplitudes for both irradiated and unirradiated conditions. Fig. 4 presents the specific simulation process and implementation pathway of the constitutive model. Furthermore, implementing the model in a finite element framework is not limited to reproducing uniaxial responses. It enables the simulation of realistic geometries, boundary conditions, and loading complexities. This is essential for extending the model to practical engineering applications where structural materials, especially those used in fusion reactors, are often subjected to multiaxial fatigue, geometric discontinuities, and non-uniform thermal fields. Developing and validating the model within a commercial finite element platform (ABAQUS via UMAT) ensures its readiness for such complex analyses. The current uniaxial simulation serves as a foundational validation step within this broader modelling framework.

In this study, the authors applied the "cycle jump" acceleration strategy, initially introduced by Zhao et al. (2024), to simulate the mechanical behaviour under LCF loading conditions. However, unlike the original approach, the authors selectively used the cycle jump method due to its limitations in accurately fitting the $k_n$ values throughout the simulation. Utilizing the cycle jump method for the entire simulation process led to inconsistencies in the $k_n$ calculation and produced variations in the values.

To address the unique characteristics of LCF, a hybrid approach is adopted. During the initial cycles, where peak stress shows significant fluctuations, the standard iterative calculation method is applied. In later stages, as peak stress stabilizes with consistent variation across cycles, the cycle-jump strategy is implemented. During this phase, the stress $\sigma$ is treated as a constant slope-based extrapolation. Specifically, the interpolation of peak stress between the $1^{st}$ and $11^{th}$ cycles is assumed to be ten times the increment between the $1^{st}$ and $2^{nd}$ cycles, allowing efficient prediction of stress evolution for cycles 1, 11, 21, etc. The parameter $k_n$ denotes the slope of the peak stress evolution in this stabilized phase and is used to extrapolate stress values across cycles. This selective application of the cycle jump method not only accelerated the computation but also maintained simulation stability. The specific strategy is depicted in Fig. 5. This approach improves both the accuracy and efficiency of the simulation, making it particularly well-suited for analysing LCF.

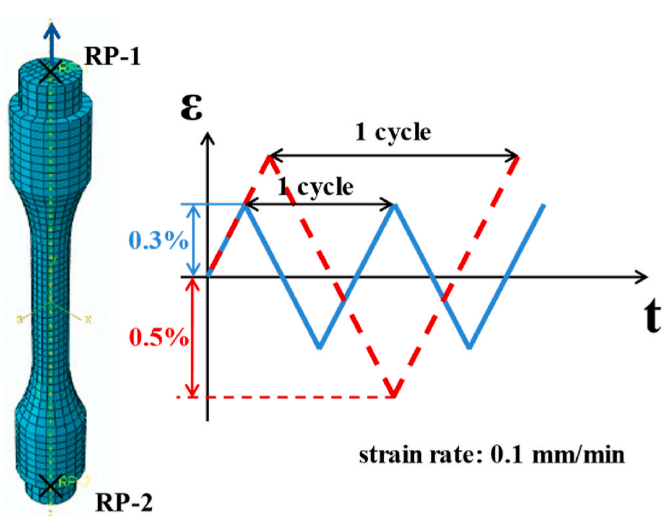


**Fig. 3.** Finite Element model and strain-controlled loading profile for LCF simulation.

## 3. Results

Fig. 6 compares the simulated and experimental (Materna-Morris et al., 2013) stress-strain hysteresis loops and peak stresses for EUROFER97 steel at 250 °C under different strain amplitudes and irradiation conditions. The figure presents three cases: (a) ±0.3 % strain amplitude, unirradiated; (b) ±0.5 % strain amplitude, unirradiated; and (c) ±0.5 % strain amplitude, irradiated to 16.3 dpa. The solid lines represent the simulation results, with the black lines depicting the complete hysteresis loops. In the initial cycles, the loops are denser due to standard iterative calculations, while in later cycles, they are more spaced out because of the cycle-jump acceleration strategy. The blue and red curves represent the hysteresis loops of the 1st and 100th cycles, respectively, while the purple line shows the evolution of peak stress throughout the cycles. The blue and red points correspond to experimental data for the hysteresis loops of the 1st and 100th cycles. The stress shown in the hysteresis loops corresponds to the axial engineering stress, which is extracted from the centre region of the specimen's gauge length. The strain represents the total axial engineering strain, defined as the applied boundary displacement divided by the original gauge length of the specimen.

Under unirradiated conditions (Fig. 6(a) and (b)), the simulation results closely align with the experimental data. For the unirradiated specimen at a ±0.3 % strain amplitude (Fig. 6(a)), the shape of the simulated hysteresis loops matches the experimental data, accurately capturing the cyclic softening trend. This suggests that the constitutive model effectively predicts the cyclic behaviour of the material at low strain amplitudes. Similarly, for the unirradiated specimen at a ±0.5 % strain amplitude (Fig. 6(b)), the simulation results fit well. Although some discrepancies occur in the kinematic hardening region, the simulation accurately reproduces the peak stress and its decreasing trend, successfully predicting cyclic softening at higher strain amplitudes. In the irradiated condition (Figure (c), ±0.5 % strain amplitude, irradiated to 16.3 dpa), the simulation remains in close agreement with the experimental data. Despite the strengthening effect caused by irradiation, the simulation accurately reflects the increase in stress levels and the trend of stress softening throughout the cycles. This shows that the developed constitutive model not only describes the cyclic behaviour under unirradiated conditions but also effectively predicts the effects of irradiation hardening on the hysteresis loops.

Overall, Fig. 6 demonstrates that the constitutive model provides a good fit with the experimental results across different strain amplitudes and irradiation conditions, validating its effectiveness in predicting the cyclic softening behaviour of EUROFER97 steel.

## 4. Discussion

Fig. 7 presents the hysteresis loops of EUROFER97 material at 250 °C and a strain amplitude of ±0.5 %, comparing the $2^{nd}$ and $100^{th}$ cycles under both irradiated and unirradiated conditions. The blue lines

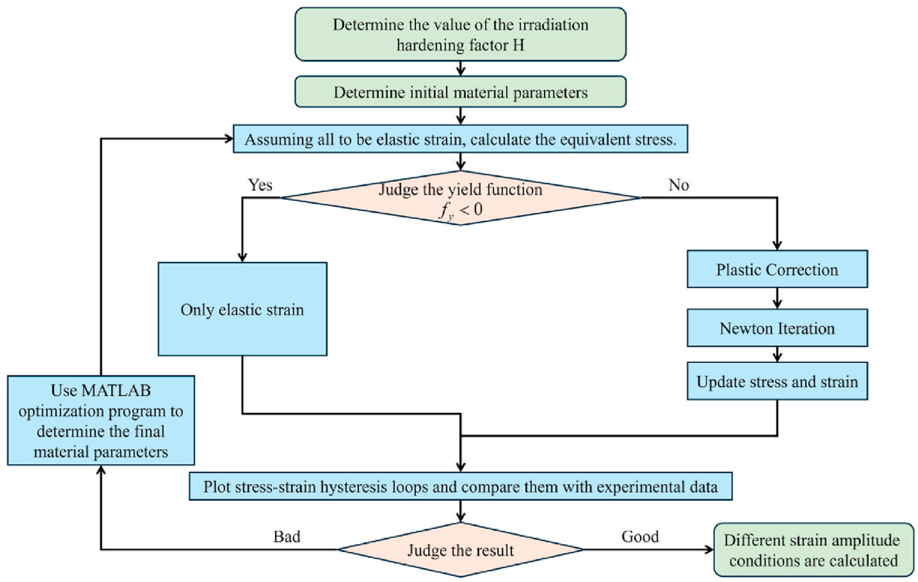


**Fig. 4.** Flowchart of constitutive model implementation in UMAT

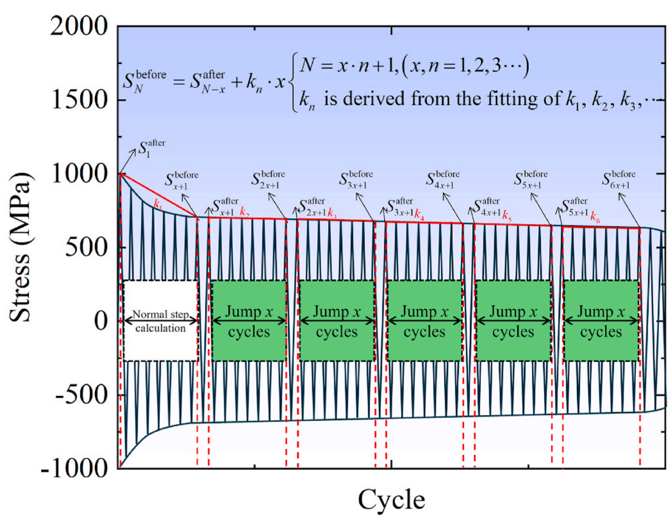


**Fig. 5.** Cycle jump strategy for accelerating LCF simulations.

represent the 2nd cycle under irradiated conditions, while the blue squares represent the 2nd cycle under unirradiated conditions. Similarly, the red lines depict the 100th cycle under irradiated conditions, and the red squares show the 100th cycle under unirradiated conditions.

Based on the analysis of Fig. 7 and relevant literature (Bhattacharya et al., 2022; Xiao, 2019; Kachko et al., 2024), irradiation significantly impacts the mechanical properties of the material. In the initial stages (2nd cycle), the irradiated material exhibits a higher peak stress due to irradiation-induced hardening. However, as the cycles progress, the irradiated material undergoes substantial softening, resulting in a notable reduction in stress by the 100th cycle. This pronounced softening is evidenced by the larger difference in peak stress between the 2nd and 100th cycles for the irradiated material compared to the unirradiated condition.

In contrast, the unirradiated material shows a more stable mechanical response, displaying only minimal softening throughout the cycles. This difference in cyclic behaviour is primarily due to the interactions between irradiation-induced defects and dislocations, which accelerate softening under cyclic loading in the irradiated material (Klimenkov et al., 2011), while the unirradiated material maintains relatively consistent mechanical properties. As a result, the initial hardening effect in the irradiated material diminishes quickly as cyclic softening becomes dominant, leading to a marked decrease in stress values over the course of 100 cycles.

Fig. 8 illustrates the relationship between irradiation dose and irradiation hardening, highlighting how the mechanical properties change with increasing neutron exposure (Lucon and Vandermeulen; Gaganidze et al.). It shows the stress-strain hysteresis loops of EUROFER97 at two different doses: 2.5 dpa and 16.3 dpa (Materna-Morris et al., 2013; Luzginova et al., 2011). It is clear that the material exhibits significantly higher stress levels at 16.3 dpa compared to 2.5 dpa, indicating a significant irradiation hardening effect at the higher dose. The simulation results fit well with the quantitative relationship between irradiation hardening and irradiation dose provided in Fig. 1.

In Section 2, the irradiation constitutive model is modified by introducing an irradiation hardening factor to take into account the irradiation hardening mechanism. The primary focus is on adjusting the initial yield stress, the saturation values and rates of kinematic hardening, and the saturation values and rates of isotropic hardening. The behaviour of the model under irradiation conditions without these modifications is discussed in detail below, comparing the hysteresis loops and cyclic softening curves before and after the modifications (Materna-Morris et al., 2013). Fig. 9 presents four cases: (a) complete modification, (b) no modification of the initial yield stress, (c) no modification of kinematic hardening and (d) no modification of isotropic hardening, each showing the hysteresis and cyclic softening curves at selected cycles.

In line with the results presented in section 3, Fig. 9-(a), which includes full modifications, accurately captures the increased initial yield stress and hardening in EUROFER97 due to irradiation. Fig. 9-(b), which lacks modifications to the initial yield stress, shows a hysteresis loop with the same yield stress as the unirradiated state, which is inconsistent with actual irradiated conditions. Under irradiation at 523 K and 16.3 dpa, the yield stress of EUROFER97 increases significantly due to the formation of dislocation loops (Kolluri et al., 2014), which impede dislocation movement and enhance the material's hardness and yield strength. Experimental data also show that the increase in yield stress after irradiation is related to the irradiation dose (Bhattacharya et al., 2021).

Fig. 9-(c), without kinematic hardening modification, shows premature stress saturation, shows peak stresses during each cycle that are lower than the actual values. Experimental data indicate that irradiation

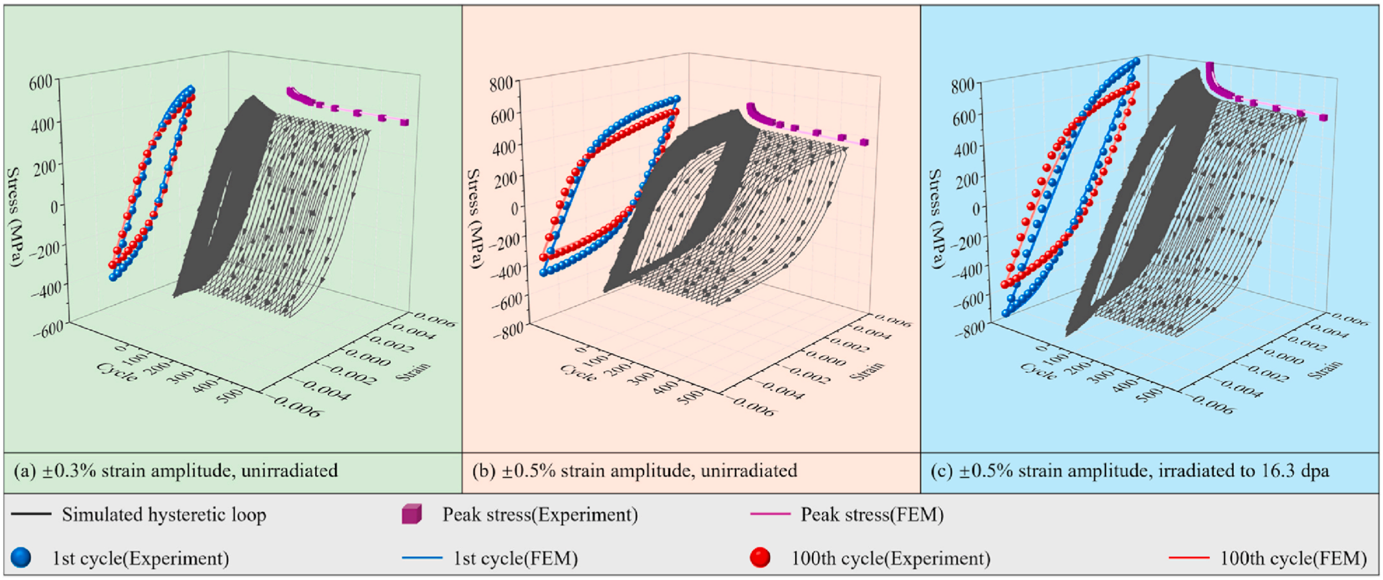


**Fig. 6.** Comparison between simulated and experimental (Materna-Morris et al., 2013) hysteresis loops and peak stress of EUROFER97 at 250 °C under different strain amplitudes and irradiation conditions: (a) ±0.3 % strain amplitude - unirradiated, (b) ±0.5 % strain amplitude - unirradiated and (c) ±0.5 % strain amplitude - irradiated to 16.3 dpa.

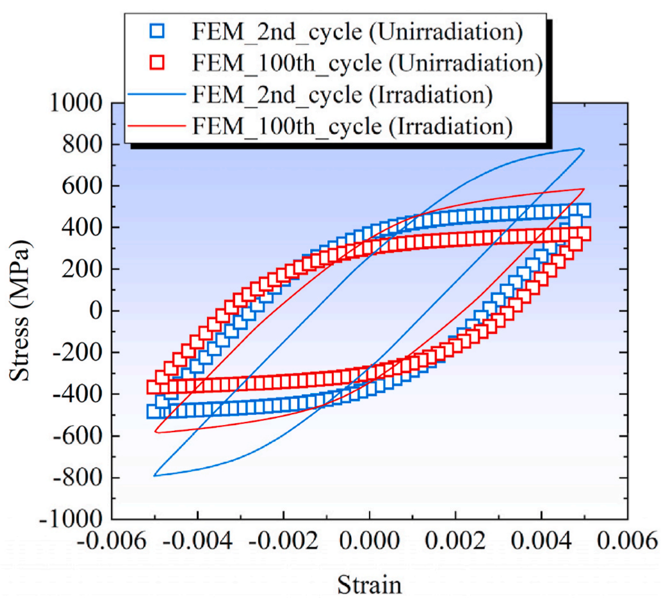


**Fig. 7.** Hysteresis loops of EUROFER97 material at 250 °C under ±0.5 % strain amplitude for the 2nd and 100th cycles in irradiated and unirradiated conditions.

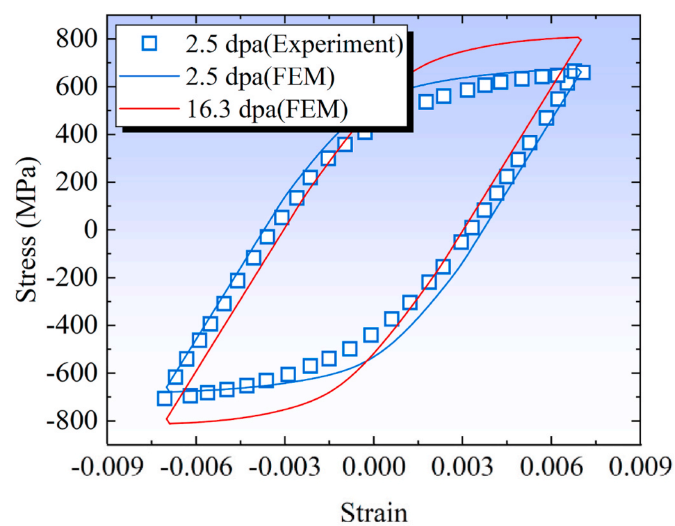


**Fig. 8.** Stress-strain hysteresis loops of EUROFER97 at different irradiation doses (2.5 dpa at 300 °C and 16.3 dpa at 250 °C) during the 1st cycle (Materna-Morris et al., 2013; Luzginova et al., 2011).

leads to an increase in both the saturation value of kinematic hardening and the hardening rate, suggesting that the material experiences greater and faster hardening during cyclic loading. The study showed that dislocation loops formed during irradiation contribute to hardening (Xiao, 2019; Was, 2007), maintaining an overall increase in the hardening rate. Consequently, both the back stress saturation value $\gamma$ and the hardening rate $\xi$ increase following irradiation.

In Fig. 9-(d), without isotropic hardening modification, stress saturation occurs prematurely during cyclic softening, leading to peak stresses in later cycles that exceed actual values. Since EUROFER97 exhibits pronounced cyclic softening in LCF tests. This effect becomes even more pronounced after irradiation. This is due to the fact that dislocations are gradually removed or rearranged as the cycles progress, thereby enhancing the softening effect (Aktaa and Petersen, 2009b).

To evaluate the applicability of the improved irradiation-informed Chaboche model across different materials, we used it to investigate the LCF behaviour of F82H ferritic/martensitic steel under irradiation. F82H is commonly used in nuclear reactor structural components due to its favourable mechanical properties and suitability for fusion environments, and its mechanical performance before and after irradiation has been extensively studied. We analyse LCF experimental data for F82H at a ±0.7 % strain amplitude, focusing on the evolution of peak stress with cycles under both irradiated (0.02 dpa at 573 K) and unirradiated conditions at room temperature (Kim et al., 2009). The experimental results show that irradiated F82H exhibits significant irradiation hardening. And given the similarity in cyclic softening behaviour between F82H and EUROFER97, we apply the improved irradiation model to predict the LCF behaviour of F82H. The procedure for identifying material parameters for F82H follows the same step-by-step approach used for

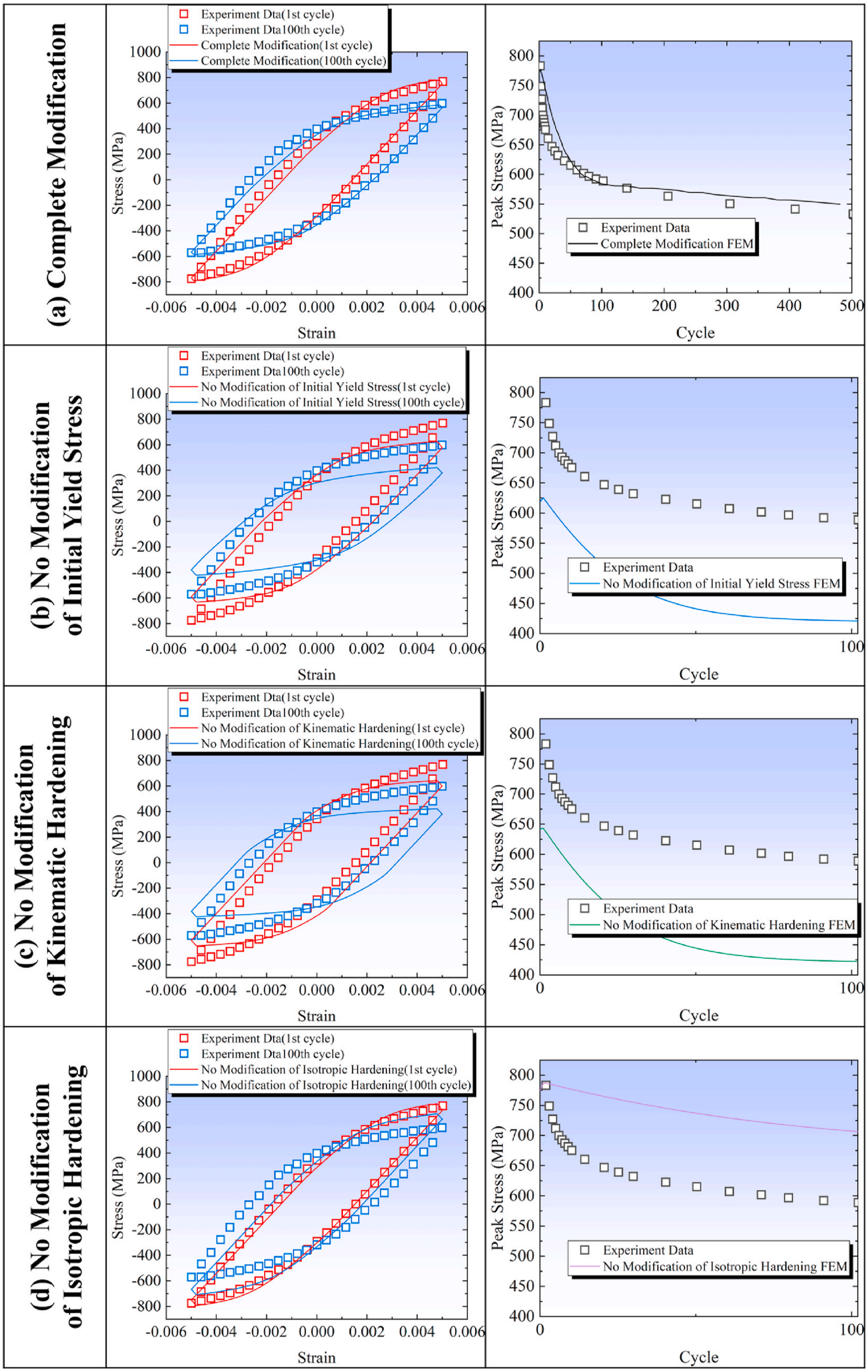


**Fig. 9.** Comparison of hysteresis loops and cyclic softening curves at 250 °C at different levels of irradiation-induced constitutive model modifications: (a) Complete modification, (b) No modification of the initial yield stress, (c) No modification of kinematic hardening and (d) No modification of isotropic hardening (Materna-Morris et al., 2013).

EUROFER97, as described in Section 2.2 and illustrated in Fig. 2. To avoid redundancy, the full calibration process is not repeated here. The key parameters used in the simulation of F82H's mechanical behaviour are provided in Table 2, with any unmentioned parameters taken from Table 1. Based on the relationship between irradiation-induced hardening and irradiation dose for F82H, as described by Aktaa et al. (Aktaa and Petersen, 2011), the irradiation factor $H$ used here is 1.15.

Fig. 10 shows the evolution of peak stress with cycle number for F82H at ±0.7 % strain amplitude under both unirradiated and irradiated conditions (Kim et al., 2009). The introduced irradiation factor effectively captures the irradiation hardening of F82H, while the original model accurately simulates the cyclic softening process. Thus, the model effectively describes the mechanical response of F82H before and after irradiation. Specifically, the predicted irradiation hardening and cyclic softening behaviours align closely with experimental data, further validating the model's applicability across different materials.

Originally developed for EUROFER97 steel, the core mechanism of the model, coupling nonlinear hardening with irradiation effects, can be extended to other materials, such as F82H. Incorporating an irradiation hardening factor allows the model to effectively capture changes in yield strength and hardening characteristics after irradiation. Validation with different materials suggests that this improved model has broad applicability for addressing irradiation hardening effects. Future studies could extend this model to evaluate its predictive capability under varying temperatures, irradiation doses, and strain conditions.

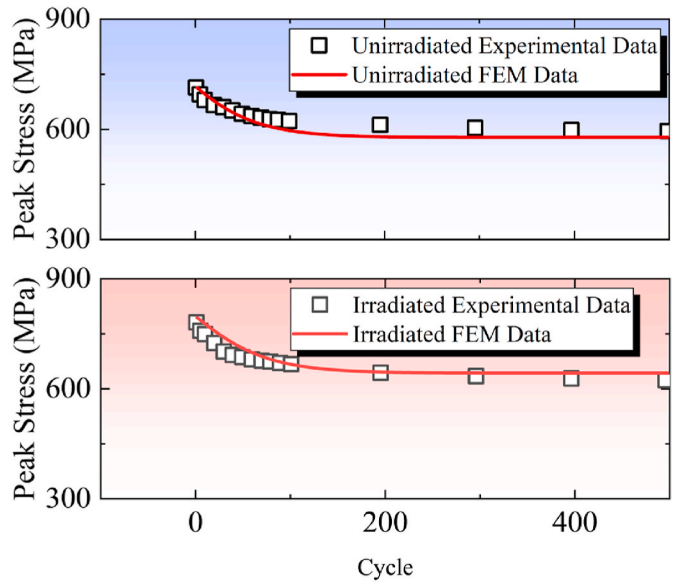


**Fig. 10.** Evolution of peak stress with cycle number for F82H under irradiated (0.02 dpa at 573 K) and unirradiated conditions at ±0.7 % strain amplitude (Kim et al., 2009).

## 5. Conclusion

The irradiation hardening behaviour of EUROFER97 steel is examined by the incorporation of an irradiation hardening factor into a modified Chaboche model to simulate its mechanical response under irradiation. The data of the simulated LCF tests are then compared with the experimental data. A set of parameters in the modified Chaboche model is calibrated using EUROFER97 experimental data to assess the model's accuracy in predicting irradiation hardening and cyclic softening effects. Based on these studies, the following conclusions are drawn:

1. The modified Chaboche model effectively predicts the stress-strain response of EUROFER97 steel, particularly under cyclic loading and LCF conditions, demonstrating good agreement with experimental data.
2. The model successfully captures the complexities of irradiation hardening, cyclic softening, and the evolution of stress-strain hysteresis loops and stress relaxation behaviour under varying strain amplitudes and irradiation doses, pointing at its robustness in predicting material response in the as-irradiated condition.
3. The model's adaptability is further demonstrated by its application to F82H ferritic/martensitic steel, potentially indicating its feasibility for extension to other structural materials applied in fusion and nuclear reactors.
4. The implementation of a hybrid acceleration strategy allows for efficient numerical simulations, while preserving prediction accuracy, achieving a balance between computational cost and precision.

## CRediT authorship contribution statement

**Jianxin Liu:** Conceptualization, Methodology, Writing – original draft. **Xiaowei Wang:** Data curation, Software. **Aleksandr Zinovev:** Writing – review & editing. **Dmitry Terentyev:** Writing – review & editing. **Lihua Wang:** Supervision, Writing – review & editing. **Magd Abdel Wahab:** Writing – review & editing, Supervision, Investigation, Conceptualization.

## Declaration of competing interest

The authors declare that they have no known competing financial interests or personal relationships that could have appeared to influence the work reported in this paper.

## Acknowledgment

This work is supported by the National Natural Science Foundation of China (Project no. 12272270) and the Shanghai Pilot Program for Basic Research.

## Data availability

Data will be made available on request.

## References

Aktaa, J., Petersen, C., 2009a. Challenges in the constitutive modeling of the thermo-mechanical deformation and damage behavior of EUROFER 97. Eng. Fract. Mech. 76, 1474–1484.
Aktaa, J., Petersen, C., 2009b. Modeling the influence of high dose irradiation on the deformation and damage behavior of RAFM steels under low cycle fatigue conditions. J. Nucl. Mater. 389, 432–435.
Aktaa, J., Petersen, C., 2009c. Deformation and lifetime prediction model for RAFM steels under creep-fatigue and high dose irradiation conditions. Wissenschaftliche Berichte FZKA 7451.
Aktaa, J., Petersen, C., 2011. Modeling the constitutive behavior of RAFM steels under irradiation conditions. J. Nucl. Mater. 417, 1123–1126.
Bacon, D.J., Osetsky, Y.N., 2002. Modelling atomic scale radiation damage processes and effects in metals. Int. Mater. Rev. 47, 233–241.
Bhattacharya, A., Chen, X., Graening, T., Geringer, J.W., Reed, J., Henry, J., et al., 2021. Irradiation hardening and ductility loss of Eurofer97 steel variants after neutron irradiation to ITER-TBM relevant conditions. Fusion Eng. Des. 173, 112935.
Bhattacharya, A., Zinkle, S.J., Henry, J., Levine, S.M., Edmondson, P.D., Gilbert, M.R., et al., 2022. Irradiation damage concurrent challenges with RAFM and ODS steels for fusion reactor first-wall/blanket: a review. J. Phys.: Energy (Calg.) 4, 034003.
Bodel, W., Butler, G., Matthews, J., 2021. Nuclear Energy for Net Zero: a Strategy for Action. District Heating, vol. 1, p. 2.
Cabet, C., Dalle, F., Gaganidze, E., Henry, J., Tanigawa, H., 2019. Ferritic-martensitic steels for fission and fusion applications. J. Nucl. Mater. 523, 510–537.
Cho, H.E., Zbib, H.M., Horstemeyer, M.F., 2021. An internal state variable Elastoviscoplasticity-Damage model for irradiated metals. J. Eng. Mater. Technol. 144.
Deo, C., Tomé, C., Lebensohn, R., Maloy, S., 2008. Modeling and simulation of irradiation hardening in structural ferritic steels for advanced nuclear reactors. J. Nucl. Mater. 377, 136–140.

Frydrych K. Modelling Irradiation Effects in Metallic Materials Using the Crystal Plasticity theory—A Review. Crystals2023.
Gaganidze E, Schneider H, Petersen C, Aktaa J, Povstyanko A, Prokhorov V, et al. Mechanical properties of reduced activation ferritic/martensitic steels after high dose neutron irradiation. Proc of 22st IAEA Fusion Energy Conference2008. p. 13-18.
Gaganidze, E., Gillemot, F., Szenthe, I., Gorley, M., Rieth, M., Diegele, E., 2018. Development of EUROFER97 database and material property handbook. Fusion Eng. Des. 135, 9–14.
Kachko, O., Puype, A., Terentyev, D., Chang, C.C., Rieth, M., Petrov, R.H., 2024. Impact of neutron irradiation on the tensile properties of advanced EUROFER97 - type steels. J. Nucl. Mater., 155176
Khraishi, T.A., Zbib, H.M., de la Rubia, T.D., Victoria, M., 2002. Localized deformation and hardening in irradiated metals: three-dimensional discrete dislocation dynamics simulations. Metall. Mater. Trans. B 33, 285–296.
Kim, S.W., Tanigawa, H., Hirose, T., Kohayama, A., 2009. Cyclically induced softening in reduced activation ferritic/martensitic steel before and after neutron irradiation. J. Nucl. Mater. 386–388, 529–532.
Klimenkov, M., Materna-Morris, E., Möslang, A., 2011. Characterization of radiation induced defects in EUROFER 97 after neutron irradiation. J. Nucl. Mater. 417, 124–126.
Kolluri, M., Edmondson, P.D., Luzginova, N.V., Berg, FAvd, 2014. A structure–property correlation study of neutron irradiation induced damage in EU batch of ODS Eurofer97 steel. Mater. Sci. Eng. A 597, 111–116.
Lin, P-d, Nie, J-f, Lu, Y-p, Shi, C-x, Cui, S-g, Cui, W-d, et al., 2024. Atomic irradiation defects induced hardening model in irradiated tungsten based on molecular dynamics and CPFEM. Int. J. Plast. 174, 103895.
Lucon E, Vandermeulen W. Overview and Critical Assessment of the Tensile Properties of Unirradiated and Irradiated EUROFER97. Belgium2007. p. 173.
Luzginova, N.V., Rensman, J., ten Pierick, P., Hegeman, J.B.J., 2011. Low cycle fatigue of irradiated and unirradiated Eurofer97 steel at 300°C. J. Nucl. Mater. 409, 153–155.
Makin, M.J., Minter, F.J., 1960. Irradiation hardening in copper and nickel. Acta Metall. 8, 691–699.
Makin, M.J., Whapham, A.D., Minter, F.J., 1962. The formation of dislocation loops in copper during neutron irradiation. Philos. Mag.: A Journal of Theoretical Experimental and Applied Physics 7, 285–299.
Marian, J., Fitzgerald, S., Po, G., 2020. Discrete dislocation dynamics simulations of irradiation hardening in nuclear materials. In: Andreoni, W., Yip, S. (Eds.), Handbook of Materials Modeling: Applications: Current and Emerging Materials. Springer International Publishing, Cham, pp. 2243–2271.
Marmy, P., 2006. Low Cycle Fatigue and creep-fatigue of Eurofer 97.
Materna-Morris, E., Möslang, A., Rolli, R., Schneider, H.C., 2011. Effect of 16.3dpa neutron irradiation on fatigue lifetime of the RAFM steel EUROFER97. Fusion Eng. Des. 86, 2607–2610.
Materna-Morris, E., Möslang, A., Schneider, H.C., 2013. Tensile and low cycle fatigue properties of EUROFER97-steel after 16.3dpa neutron irradiation at 523, 623 and 723K. J. Nucl. Mater. 442, S62–S66.
Melton, S., Wiffen, F., Kato, Y., 2020. Fusion Materials Research at Oak Ridge National Laboratory in Fiscal Year 2019.
Reali, L., Dudarev, S.L., 2024. Finite element models for radiation effects in nuclear fusion applications. Nucl. Fusion 64, 056001.
Tavassoli, A.-A., Diegele, E., Lindau, R., Luzginova, N., Tanigawa, H., 2014. Current status and recent research achievements in ferritic/martensitic steels. J. Nucl. Mater. 455, 269–276.
Tong, J., Zhan, Z.L., Vermeulen, B., 2004. Modelling of cyclic plasticity and viscoplasticity of a nickel-based alloy using chaboche constitutive equations. Int. J. Fatig. 26, 829–837.
Van Der Giessen, E., Schultz, P.A., Bertin, N., Bulatov, V.V., Cai, W., Csányi, G., et al., 2020. Roadmap on multiscale materials modeling. Model. Simulat. Mater. Sci. Eng. 28, 043001.
Wang, X., Zhang, T., Zhang, W., Wahab, M.A., Gong, J., 2021. An improved unified viscoplastic model for modelling low cycle fatigue and creep fatigue interaction loadings of 9–12%Cr steel. Eur. J. Mech. Solid. 85, 104123.
Was, G.S., 2007. Fundamentals of Radiation Materials Science: Metals and Alloys. Springer.
Windsor, C., Keilhacker, M., Lawson, J.D., Pert, G.J., Robinson, D.C., Ehrlich, K., 1999. The development of structural materials for fusion reactors. Philos. Trans. R. Soc. London, Ser. A: Math. Phys. Eng. Sci. 357, 595–623.
Xiao, X., 2019. Fundamental mechanisms for irradiation-hardening and embrittlement: a review. Metals 9.
Yamamoto, T., Odette, G.R., Kishimoto, H., Rensman, J.-W., Miao, P., 2006. On the effects of irradiation and helium on the yield stress changes and hardening and non-hardening embrittlement of ~8Cr tempered martensitic steels: compilation and analysis of existing data. J. Nucl. Mater. 356, 27–49.
Zahran, H., Zinovev, A., Terentyev, D., Wang, X., Abdel, Wahab M., 2024. Experimental investigation and constitutive material modelling of low cycle fatigue of EUROFER97 for fusion applications. J. Nucl. Mater. 588, 154809.
Zhang, K., Aktaa, J., 2020. Ratcheting and fatigue behavior of Eurofer97 at high temperature, part 2: modeling. Fusion Eng. Des. 152, 111426.
Zhang, S.-L., Xuan, F.-Z., 2017. Interaction of cyclic softening and stress relaxation of 9–12% Cr steel under strain-controlled fatigue-creep condition: experimental and modeling. Int. J. Plast. 98, 45–64.
Zhao, Q., Abdel, Wahab M., Ling, Y., Liu, Z., Wang, D., 2024. Fatigue crack propagation of AA2024 alloy under texture control using crystal plasticity coupled with accelerated cyclic cohesive zone model. Eng. Fract. Mech. 296, 109819.
Zinkle, S.J., Boutard, J.L., Hoelzer, D.T., Kimura, A., Lindau, R., Odette, G.R., et al., 2017. Development of next generation tempered and ODS reduced activation ferritic/martensitic steels for fusion energy applications. Nucl. Fusion 57, 092005.